2011 American Control Conference
on O'Farrell Street, San Francisco, CA, USA
June 29 - July 01, 2011

# Effective strategies for real time hybrid simulation of near seismic collapse response of moment resisting frames

M. Leclerc, M. Molinari, N. Bouaanani, R. Tremblay, P. Leger and O. Bursi

*Abstract*— **Reliable assessment of seismic performance of structural systems requires accurate and robust simulation techniques that can efficiently predict inelastic response in the large deformation range, up to structural collapse. This paper presents a real-time dynamic substructuring (RTDS) test program carried out on steel moment resisting frames (MRF) tested up to near collapse. A single-story, industrial building with steel MRFs at perimeter was examined applying the Loma Prieta earthquake record. Columns were pinned at their bases, while full stiffness and resistance was retained at beam-to-column joints. The physical substructure included only one column that was installed in the inverted position i.e. clamped at the base and pinned at the top: in this way only one lateral degree of freedom was involved in physical tests. The other column, the beam, building masses, gravity loads and damping forces were included in the numerical substructure. Time integration was performed using a variant of a Rosenbrock-W scheme implemented into the MathWorks's Simulink and XPC target computer environment. The tangent stiffness matrix of the structure was evaluated using different numerical strategies including data smoothing and filtering. Control techniques with constant or adaptive delay compensation for the feed-forward filter were implemented. The obtained results are compared and discussed to highlight the effect on structural response predictions. As a result, RTDS tests appear to be effective in the prediction of near collapse seismic response of steel frames, provided that robust numerical strategies are implemented.**

## I. INTRODUCTION

Evaluation of the collapse capacities or margin against collapse under seismic ground motions has become a generally accepted method to assess the capacity of seismic resistant systems to safely withstand ground motions [1]. Accordingly, incremental dynamic analyses [2] are performed to determine collapse points. The method heavily depends on accurate and reliable numerical simulation techniques that can efficiently predict inelastic seismic response in the large deformation regions, up to structural collapse. Hybrid simulation of the seismic collapse response of portal frames were investigated [3], but tests were performed at a rate significantly (31 times) slower than real time. In this study, real-time dynamic substructuring (RTDS) testing was conducted to examine the control and signal filtering techniques that are required to effectively carry out real time hybrid simulations of the near collapse seismic response of steel moment-resisting frames.

RTDS testing is based on a substructuring technique where the investigated system is split into: (i) a physical substructure consisting of a critical part or component tested experimentally under dynamic forcing, and (ii) a numerical substructure modeling the reaction of the remaining part of the system [4]. To realistically emulate the behavior of the whole system during dynamic excitation, control strategies and numerical algorithms are conceived so that physical and numerical substructures interact in real time. A significant advantage of RTDS testing is that velocity dependant phenomena such as strain rate effects on material response can be accounted for in the simulation.

In this paper robust strategies to perform RTDS tests for the prediction of near collapse seismic response are proposed, compared and validated. The structural model, the adopted hybrid testing configuration and the RTDS testing environment are described. The test program included preliminary cyclic quasi-static and several RTDS tests, repeated with different numerical methods. As a result, the influence of delay compensation techniques as well as the effects of filtering and smoothing feedback signals are detected and commented upon.

## II. STRUCTURAL MODEL AND TESTING ACTIVITY

The structural model of the tested moment resisting frame (MRF) is a one-third scale of the perimeter MRF of the single-story industrial building shown in Fig 1. In the

Manuscript received September 22, 2010. This work was supported in part by the Government of Quebec, Canada, through the FQRNT Center of Excellence program and by the Government of Canada through the Canadian Research Chair program.

M. Leclerc is with the Department of Civil, Geological and Mining Engineering, Ecole Polytechnique, Montreal, QC Canada H3C 3A7 (e-mail: martin.leclerc@polymtl.ca).

M. Molinari is with the Department of Mechanical and Structural Engineering, University of Trento, 38050 Trento, Italy (e-mail: marco.molinari@ing.unitn.it).

N. Bouaanani is with the Department of Civil, Geological and Mining Engineering, Ecole Polytechnique, Montreal, QC Canada H3C 3A7 (e-mail: najib.bouaanani@polymtl.ca).

R. Tremblay is with the Department of Civil, Geological and Mining Engineering, Ecole Polytechnique, Montreal, QC Canada H3C 3A7 (phone: 514-340-4711; fax: 514-340-5881; e-mail: robert.tremblay@polymtl.ca).

P. Leger is with the Department of Civil, Geological and Mining Engineering, Ecole Polytechnique, Montreal, QC Canada H3C 3A7 (e-mail: pierre.leger@polymtl.ca).

O. Bursi is with the Department of Mechanical and Structural Engineering, University of Trento, 38050 Trento, Italy. (e-mail: oreste.bursi@ing.unitn.it).

prototype structure, the MRFs consisted of two identical W310x158 (metric I steel shape) columns pinned at their bases and rigidly connected at their upper ends to a W610x241 beam; full stiffness and resistant beam-to-column connection was conceived. Following the RTDS method, only one of the MRF columns was physically tested in the laboratory, whereas the other column and the beam, masses (m), gravity loads (P), damping and P-Δ forces were all included in the numerical substructure. This choice was motivated by the fact that inelastic deformations concentrate in the columns only, owing to the weak column–strong beam design adopted for the single-story frames. Fig. 2(a) illustrates the tested frame and the degrees of freedom (DOFs), as well as the numerical and physical substructures. A one third reduced scale model was tested in the laboratory: the W100x19 steel profile (metric I steel shape) used for column specimens meets the geometric similitude requirements.

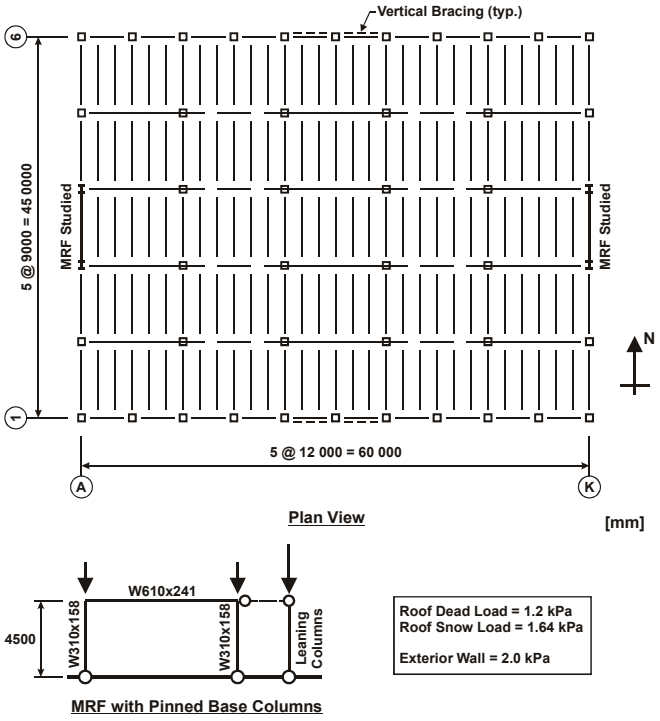


Fig. 1. Plan view of the prototype industrial building and elevations of the studied MRF.

Figures 2(b) and 3 show the testing set-up used to conduct the quasi-static cyclic and RTDS tests. Experimental displacements were imparted by a 100 kN high performance dynamic actuator, having its weight balanced with a suspended equivalent mass to minimize the shaft friction. The tested columns were anchored at their base through thick steel plates specifically designed to represent a fixed end condition. The column experimental stiffness resulted approximately 0.73 kN/mm.

To test the reliability of different experimental techniques, the axial stiffness of the beam was considered in this 4 DOFs, symmetrical model: the two modes of vibration of 1.04 Hz (flexural mode, governed by columns deformability) and 26.1 Hz (axial beam vibration) corresponded to an overall numerical mass of 27431 kg. No other modes of vibration were included in the numerical model since no rotational inertia was included in the mass matrix. The oil column frequency was experimentally measured at 15.5 Hz.

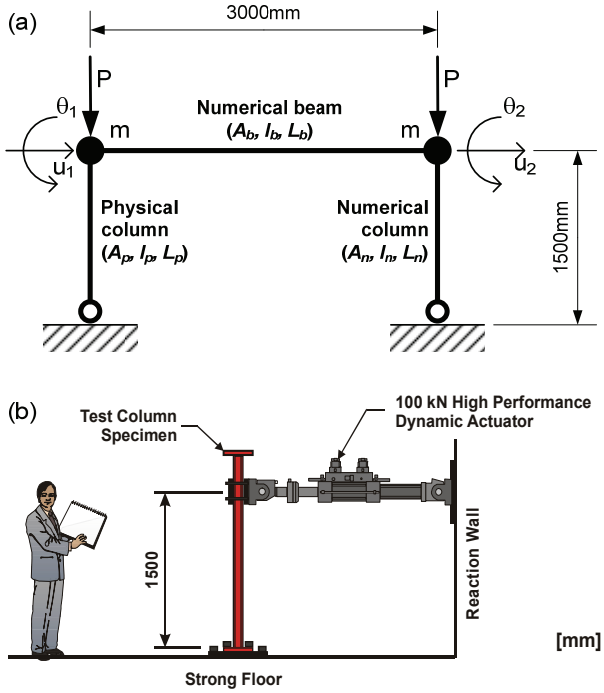


Fig. 2. MRF tested: (a) MRF studied, degrees of freedom (DOFs) and numerical and physical substructures, (b) Test configuration, physical column and dynamic actuator.

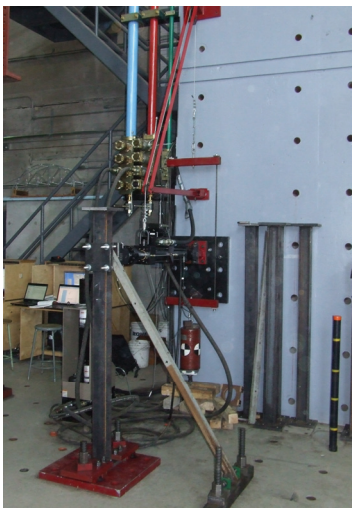

Fig. 3. Experimental set-up

Following a canonical approach, three actuators – two vertical, placed at a certain centre-distance and acting at the edges of a rigid horizontal beam connected to top edge of

the column, plus an horizontal one - should be used to completely model the structural continuity, decoupling the physical and numerical substructures. However, the test control could be problematic for the limited axial deformability of the column.

In the approach followed in this research the axial force is neglected, thus loosing small P-δ effects like local section instability: this simplification is justified since axial load is not significant in the considered single-storey building. The pinned-base MRF column was tested following an inverted configuration with the fixed end at the bottom and the pinned end at the top, coincident with the swivel of the horizontal actuator. However, a correction in the actuator displacement was required to account for the beam rotation $\theta_1$ at the ends of the frame beam. As a consequence, the online computation of $\theta_1$ required the development of specific numerical techniques, described hereafter.

The joint rotation $\theta_1$ (Fig. 2 (a)) was computed in real time to correct the imposed actuator displacement command $u_{ac}$:

$$u_{ac}(t_k) = u_1(t_k) - \theta_1(t_{k-1}) L_p \tag{1}$$

in which $L_p$ denotes the height of the tested column. The nodal forces and displacements are related by:

$$\begin{bmatrix} F_1 \\ F_2 \\ M_1 \\ M_2 \end{bmatrix} = \mathbf{K} \begin{bmatrix} u_1 \\ u_2 \\ \theta_1 \\ \theta_2 \end{bmatrix} \tag{2}$$

where the stiffness matrix $K$ of the MRF is given by:

$$\mathrm{K} = \begin{bmatrix} \frac{3EI_p}{L_p^3} + \frac{EA_b}{L_b} & -\frac{EA_b}{L_b} & -\frac{3EI_p}{L_p^2} & 0 \\ -\frac{EA_b}{L_b} & \frac{3EI_n}{L_n^3} + \frac{EA_b}{L_b} & 0 & -\frac{3EI_n}{L_n^2} \\ -\frac{3EI_p}{L_p^2} & 0 & \frac{4EI_b}{L_b} + \frac{3EI_p}{L_p} & \frac{2EI_b}{L_b} \\ 0 & -\frac{3EI_n}{L_n^2} & \frac{2EI_b}{L_b} & \frac{4EI_b}{L_b} + \frac{3EI_n}{L_n} \end{bmatrix} \tag{3}$$

Terms of stiffness matrix were updated online to obtain physical column end force $F_1$ and bending moment $M_1$ using:

$$F_1 = \left( \frac{EA_b}{L_b} + \frac{3EI_p}{{L_p}^3} \right) u_1 - \frac{EA_b}{L_b} u_2 - \frac{3EI_p}{{L_p}^2} \theta_1 \tag{4}$$

$$M_1 = \frac{-3EI_p}{{L_P}^2} u_1 + \left( \frac{4EI_b}{L_b} + \frac{3EI_p}{L_p} \right) \theta_1 + \frac{2EI_b}{L_b} \theta_2 \tag{5}$$

in which the stiffness $EI_p$ of the physical column was updated by appropriate algorithms during the test using the actuator load-cell and displacement transducer (LVDT).

The stiffness of the numerical column $EI_n$ was computed using a Giuffrè-Menegotto-Pinto (GMP) model [5] calibrated to reproduce the physical column hysteretic behavior using short and long quasi-static cyclic test protocols shown in Fig. 4. An almost perfect overlapping was obtained, as shown in Figs. 5 and 6.

Mass and stiffness proportional Rayleigh damping corresponding to 5% of critical damping in the first and second mode of vibration was used in the model.

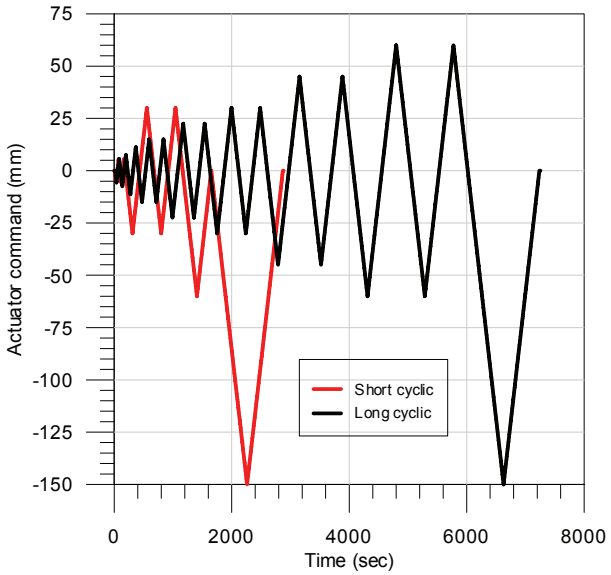


Fig. 4. Displacement protocol imposed in quasi-static cyclic tests.

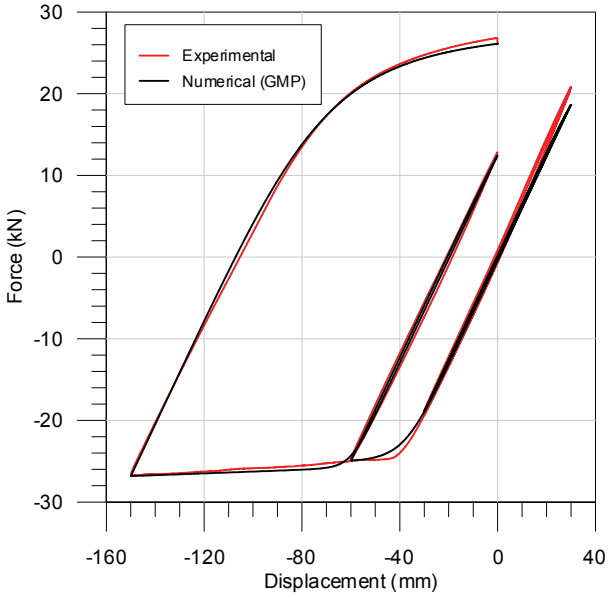


Fig. 5. Short quasi-static cyclic hysteretic response.

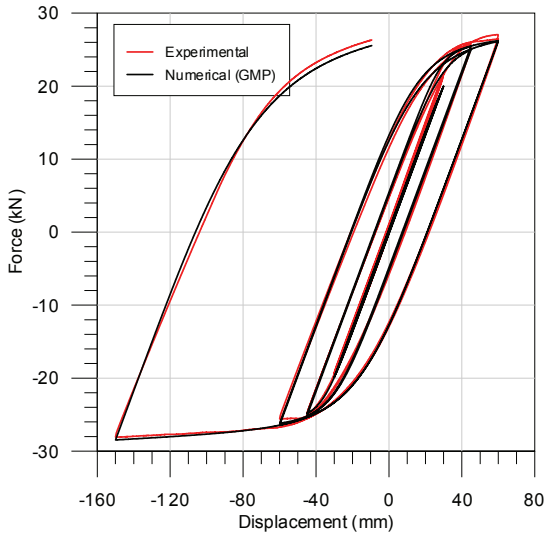


Fig. 6. Long cyclic hysteretic response.

The RTDS test program consisted of 10 experiments on 5 columns subjected to the 1989 Loma Prieta earthquake record (Stanford University, 360°) illustrated in Fig. 7: non-linear tests followed preliminary elastic ones. According to similitude requirements, the time scale of the earthquake was reduced by a factor of $1/\sqrt{3}$. Moreover, the amplitude was scaled by a factor of 2.5, which corresponded to the predicted collapse level.

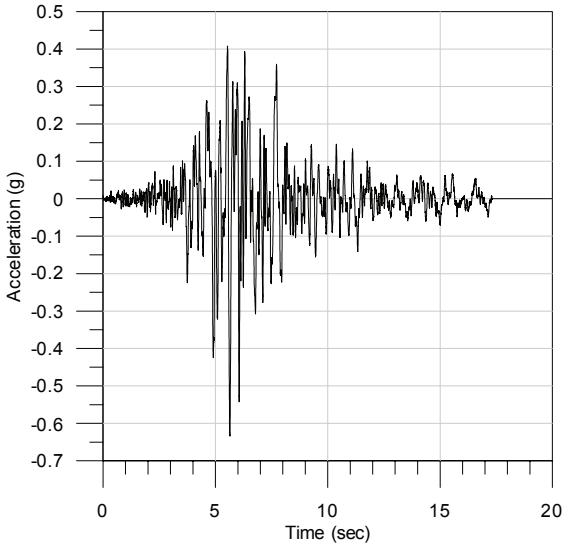


Fig. 7. 1989 Loma Prieta earthquake record used for RTDS tests.

## III. RTDS TESTING ENVIRONMENT, REAL TIME CONTROL SYSTEM AND SOLUTION ALGORITHM

### A. Testing environment

RTDS tests were carried out in the Structural Engineering Laboratory of École Polytechnique de Montréal. The physical column substructure was tested using a dynamic double ended MTS servo-hydraulic actuator, with ±127 mm stroke and ±100 kN capacity. The 227 l/min two-stage servovalve was driven using the real-time MTS structural PID control system connected to a real time PC via Scramnet shared memory where the integration scheme was embedded using MathWorks Simulink, MathWorks Real-Time Workshop and MathWorks XPC target [6]. The time step of 1/1024 s, corresponding to the controller internal clock, was used in all tests.

### B. Feed-forward vectors

The delay, $\tau$, between the command and feedback in the actuator displacement was compensated by using either a first order or a second order feed-forward prediction vector built-in the Simulink model:

1st order:

$$\mathbf{FF}_1 = [1 + ff \quad ; \quad -ff] \tag{6}$$

2nd order:

$$\mathbf{FF}_2 = \left[1 + ff + \frac{ff^2}{2} \quad ; \quad -ff - ff^2 \quad ; \quad \frac{ff^2}{2}\right] \tag{7}$$

where

$$ff = \frac{\tau}{\Delta t} \tag{8}$$

in which $\Delta t$ denotes the controller time step.

The corrected actuator displacement command $u_{ac}^c$ at time $t$ is the product of the feed-forward prediction vector and the displacement command vector $u_{dc}$:

1st order:

$$u_{ac}^c(t) = \mathbf{FF}_1 \cdot [u_{dc}(t); \quad u_{dc}(t - \Delta t)]^T \tag{9}$$

2nd order:

$$u_{ac}^c(t) = \mathbf{FF}_2 \cdot [u_{dc}(t); \quad u_{dc}(t - \Delta t); \quad u_{dc}(t - 2\Delta t)]^T \tag{10}$$

In Fig. 8, the amplitude magnification is plotted against the frequency for the two feed-forward filters for a delay of 0.037 sec. Fig. 9 presents the phase angles for both feed-forward techniques for the same delay. The second order feed-forward filter exhibits less amplitude magnification under 10 Hz while the phase angle remains almost linear. A linear phase angle corresponds to a constant delay over the frequency range, which means that all the actuator command frequencies below 10 Hz are synchronized after the application of the second order feed-forward filter. Moreover, a linear magnification equal to unity over a longer frequency range is more suited to avoid overshooting of the command for higher frequencies. For all the aforementioned reasons, the second order feed-forward filter provides a superior control, thus improving the experimental accuracy.

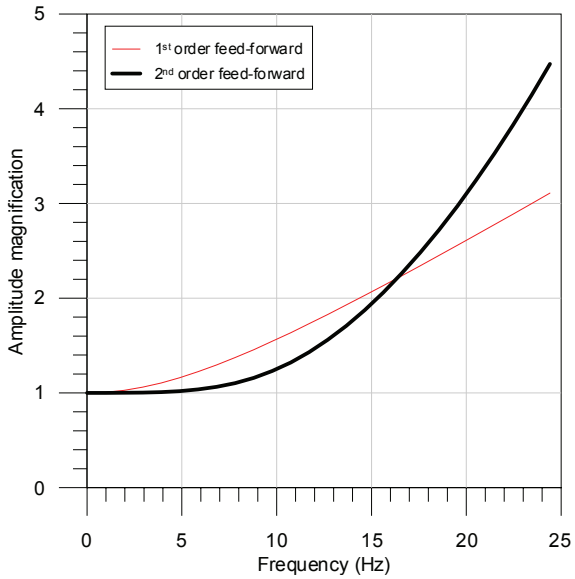


Fig. 8. Amplitude magnification of the feed-forward filter vs. frequency.

The second order feed-forward filter exponentially amplifies signal amplitude and nonlinearly distorts phase angle above 10 Hz. Since the oil column resonance is at 15.5 Hz and the second mode of vibration is at 26.1 Hz, both of these problems are prevented by applying appropriate filtering thus removing spectral content above 10 Hz.

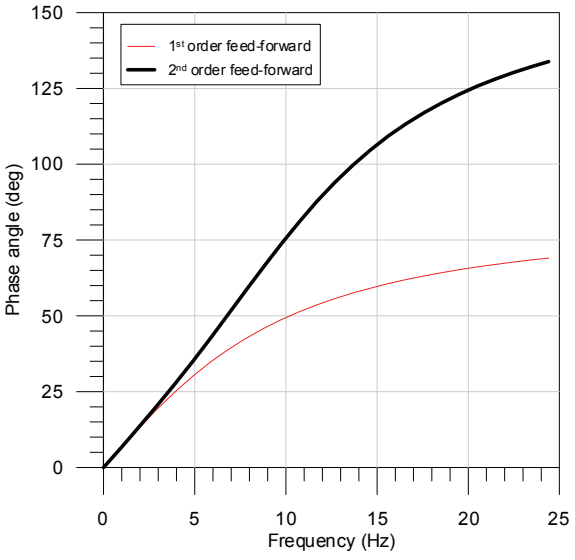


Fig. 9. Phase angle of the feed-forward filter vs. frequency.

### C. *Solution algorithm and integration method*

The RTDS tests were conducted using a variant of the Rosenbrock-W integration method [7]. In this variant, an approximation of the Jacobian matrix that accounts for the properties of both the physical and numerical substructures is used throughout the analysis process. Only an initial estimate of the stiffness and damping properties of the physical components is required. It was demonstrated that the method is unconditionally stable provided that specific conditions are fulfilled and that the order accuracy can be maintained in the nonlinear regime without involving any matrix inversion while testing. The method also features controllable numerical energy dissipation characteristics and explicit expression of the target displacement and velocity vectors. The Rosenbrock-W integration method was also verified through RTDS tests of SDOF and MDOF structures with linear and nonlinear physical substructures [8].

## IV. NUMERICAL STRATEGIES FOR ROBUST CONTROL IN NEAR COLLAPSE RTDS TESTS

The RTDS tests were conducted using different numerical strategies and the obtained results are compared in this section to highlight the effects of these strategies on structural response predictions up to near collapse.

### A. *Adaptive delay compensation and feed-forward vectors*

Both the actuator displacement command and feedback signals time histories are plotted in Fig. 10 for a near collapse RTDS test, where a first–order feed-forward vector with a constant delay was used. The actuator feedback overshooted the actuator command and a significant delay between the two signals was observed in some portions of the time-history response. In fact, it was not possible to accurately tune the PID parameters of the actuator using the first order feed-forward vector; this led to either an overshot of the command signal, with nearly no delay between the signals, or to an appropriate amplitude control with a delay where the feedback signal was lagging behind the command signal.

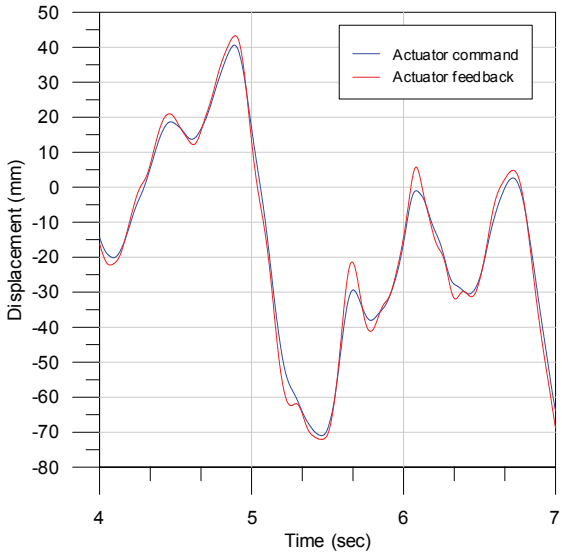


Fig. 10. Actuator displacement command and feedback signals in near collapse RTDS test using first order feed-forward vector and a constant delay.

Moreover, both the actuator displacement command and feedback signals are plotted in Fig. 11 for a near collapse RTDS test where a second order feed-forward vector was used with adaptive delay compensation technique. A constant delay compensation approach resulted in a less accurate compensation for very small displacements as the delay increases exponentially when approaching zero oscillation amplitudes. The adaptive delay compensation technique used in this test program is based on the root mean square (RMS) of the actuator displacement [8]. The delay measured during a near collapse RTDS test vs. the actuator displacement is plotted in Fig. 12.

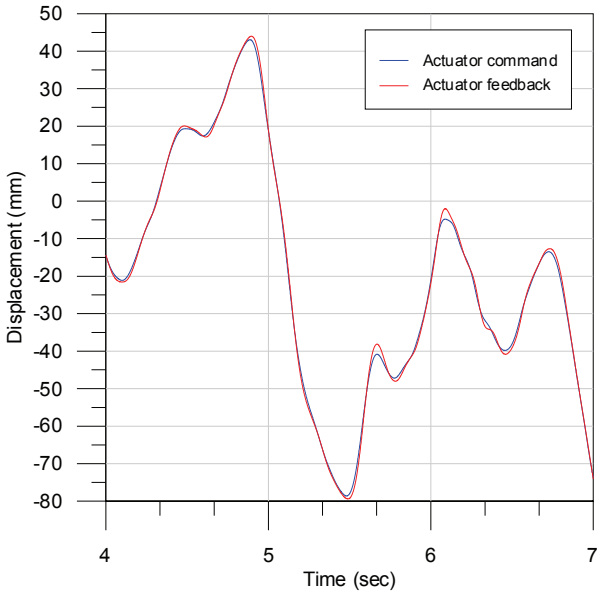


Fig. 11. Actuator displacement command and feedback signals in near collapse RTDS test using second order feed-forward vector and an adaptive delay compensation.

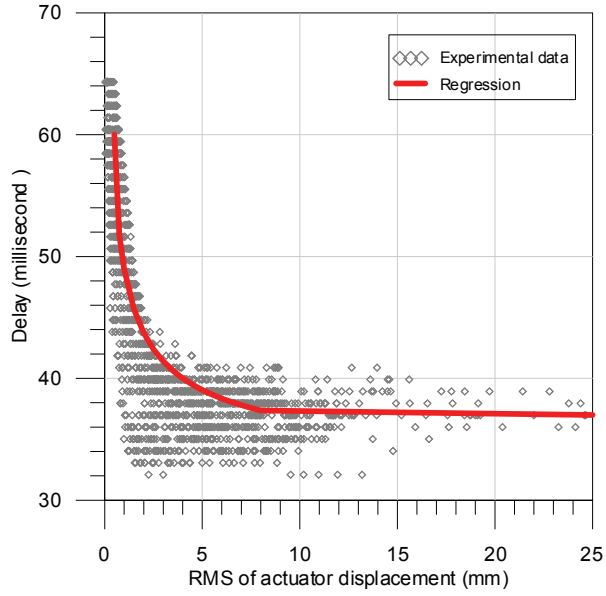


Fig. 12. Experimental data from a near collapse RTDS and the resulting regression for the delay estimation.

From these experimental data, the delay was estimated from regression via:

$$\tau = 31 + \frac{18}{\sqrt{RMS}}; \qquad 37 \le \tau \le 60 \quad (in\ ms) \tag{11}$$

Since the delay is influenced by the actuator, PID settings, electronics and filters, a different fitting has to be computed if one of these influencing variable is modified.

## B. *Stiffness updates*

The computation of the flexural stiffness of the physical column in real-time was the most critical challenge encountered in RTDS tests, in order to ensure the stability of the numerical solution: the stiffness computation affects the estimation of rotation and, trough (1), the actuator displacement command and the system stability itself. An effective technique was the implementation of Broyden [9] formula:

$$\mathbf{K}_n = \mathbf{K}_{n-1} + \frac{\left(\Delta\mathbf{r}_n - \mathbf{K}_{n-1}\Delta\mathbf{x}_n\right)\left(\Delta\mathbf{x}_n\right)^T}{\left(\Delta\mathbf{x}_n\right)^T \Delta\mathbf{x}_n} \tag{12}$$

where $\mathbf{K}_{n-1}$ and $\mathbf{K}_n$ are the stiffness matrices at time steps $n$-1 and $n$, respectively, while $\Delta\mathbf{r}_n$ and $\Delta\mathbf{x}_n$ are the corresponding incremental force and displacement vectors. Owing to signal noise, the method resulted in a very scattered stiffness estimation and the system was prone to instability. Following [10], the numerical stability was obtained by updating the tangent stiffness of the physical column only in integration time steps in which displacements or force increments were sufficiently large compared to the actuator noise level. In [10], the recommended threshold value is the greater between: (i) 10 times the RMS value of the displacement noise, or (ii) a value that results in a force (using the initial stiffness) 10 times greater than the RMS value of the force noise. In this work, much larger values were necessary reaching as much as 3 mm for the displacement increment, i.e., 750 times the RMS value of the displacement noise, and 2 kN for the force increment, i.e. 130 times the RMS value of the force noise.

The use of such larger values allows avoiding the use of high order low-pass filters that would adequately remove noise but also increase the overall delay of the system. A higher delay involves the increase of the proportional gain on the PID controller which, in turn, results in overshooting of the actuator displacement feedback signal. Force and displacement triggers were determined by minimizing the square of the error between the numerical and the physical stiffness.

Figure 13 shows the time history of the physical column stiffness during a near collapse RTDS test via the Broyden updating technique with the larger displacement and force

triggers described above.

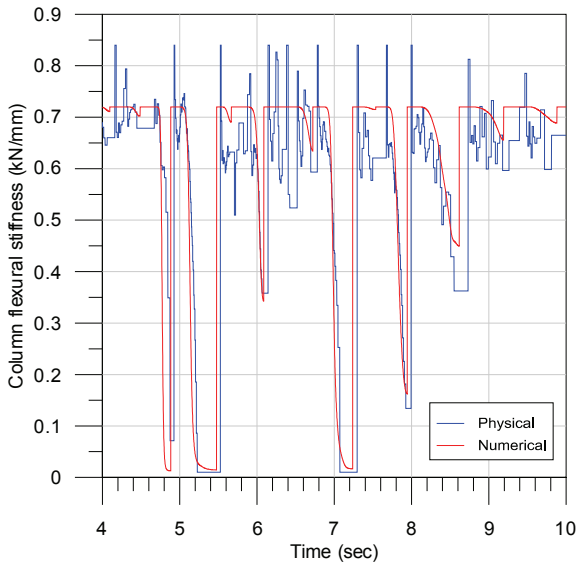


Fig. 13. Time variation of the physical and the numerical column stiffness during a near collapse RTDS test.

The stiffness of the numerical column as computed from the GMP model calibrated against the quasi-static cyclic test results is also plotted for comparison.

### C. *Low-pass filtering and signal smoothing*

Structural systems commonly contains high frequency phenomena (f > 10 Hz) like oil column resonance, higher modes of vibration or noise from instruments. Additionally, the second order feed-forward prediction vector further amplifies the signal in the high frequencies range. In order to minimize these spurious frequencies, Low-Pass Filters (LPF) and smoothing techniques were implemented. LPF was simultaneously applied to force and displacement signals, thus keeping all signals in phase; smoothing doesn't introduce any phase lag. In this experimental program, a 2nd order 8 Hz Butterworth LPF was used, of the Infinite-duration Impulse Response (IIR) filter type: conversely, Finite-duration Impulse Response (FIR) filters generally require a much higher order to achieve a comparable level of performance. Correspondingly, the delay of these filters is typically much greater compared to equal performance IIR filters. The threshold frequency (8 Hz) is low enough to prevent disturbances from oil column resonance and from feed-forward filter, in the meantime being greater enough than the first natural frequency (1.04 Hz) to retain the significant spectral content.

LPFs alone were not sufficient to handle noise problems, therefore smoothing functions were coupled to LPF: in this study, the least squares linear regression was used. In detail, the smoothing function was computed referring to six signal values, starting at the actual time step *t* and going back in time at fixed intervals. The resulting linear equation was then used to re-compute the new signal value at time *t*. For displacements, a time interval up to 19.5 ms (20 time steps) was used: the appropriate intervals were selected by minimizing the square of the error between the computed stiffness of the physical column and that of the numerical column.

To emphasize the improvement gained by filtering and smoothing, force vs displacement hysteretic diagrams of RTDS tests with and without them are shown. In Fig. 14, the blue line is relevant to a test with both LPF and smoothing, and the gray line to a test with the smoothing only: in the last case, after load reversal, the physical stiffness computation became unstable, considerably increasing higher frequency content in the response.

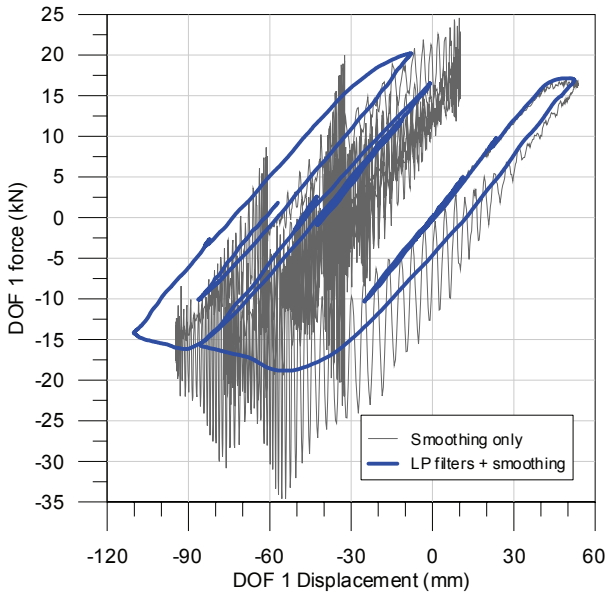


Fig. 14. Force vs displacement curves illustrating the effect of removing LPF on RTDS test results.

In Fig. 15 the blue line, relevant to test with both LPF and the smoothing techniques, is overlapped to response of a test in which only LPF was applied. From these diagrams, the removing of smoothing appears less significant than removing LPF but still increases high frequency fluctuations in the response.

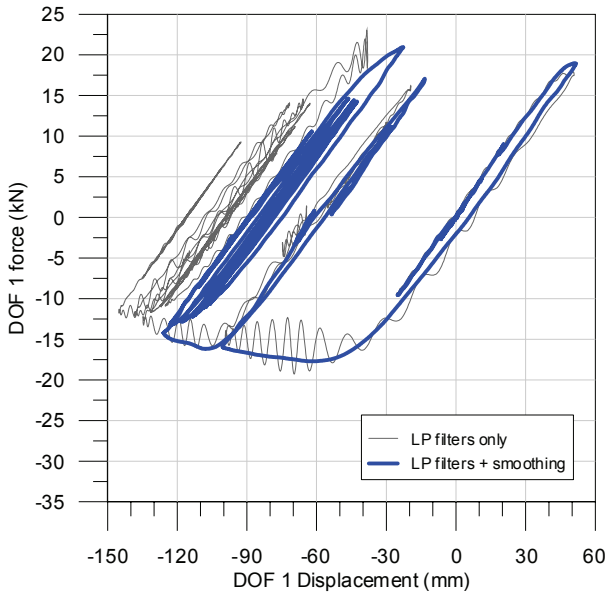


Fig. 15. Force vs displacement curves illustrating the effect of removing smoothing on RTDS test results.

## CONCLUSION

An RTDS test program was carried out on a flexible steel moment resisting frame subjected to significant inelastic, near collapse response to investigate the influence of various techniques on the quality of the simulations. The structure response was characterized by significant variations in lateral stiffness, particularly at load reversals. The physical model included an inverted cantilever column specimen and involved only one translational degree of freedom. This simple and cost effective hybrid simulation configuration required that the kinematic rotational response at the beam-to-column joint be determined based on the measured flexural stiffness of the test columns to enforce displacement compatibility. Satisfactory results were obtained by making use of delay compensation techniques as well as a combination of low-pass filter and linear regression smoothing techniques to remove parasitic high frequencies.

## ACKNOWLEDGMENT

The authors wish to thank Prof. Charles-Philippe Lamarche of the University of Sherbrooke for his valuable technical input in the test program. Prof. Antonio Agüero Ramón-Llin, from the Departamento de Mecánica de los Medios Continuos y Teoría de Estructuras, Universidad Politécnica de Valencia, conducted preliminary numerical simulations in preparation of the test program described in this paper.

## REFERENCES

[1] ATC, FEMA P695, *Quantification of Building Seismic Performance Factors*. Applied Technology Council, Redwood City, CA, 2009.

[2] D. Vamvatsikos, and C.A. Cornell, "Incremental Dynamic Analysis," *Earthquake Engineering and Structural Dynamics*, Vol. 31, no. 3, pp. 491-514, 2002.

[3] A. Schellenberg, T. Y. Yang, S. A. Mahin, and B. Stojadinovic, "Hybrid simulation of structural collapse," *Proc. of 14th World Conf. on Earthquake Eng.*, Beijing, China, Paper no. S16-02-004, 2008.

[4] K.H. Nakashima, and E. Takaoka, "Development of real-time pseudo dynamic testing," *Earthquake Engineering and Structural Dynamics*, Vol. 21, no. 1, pp. 79-92, 1992.

[5] M. Menegotto, and P.E. Pinto, "Method of analysis for cyclically loaded reinforced concrete plane frames including changes in geometry and non-elastic behavior of elements under combined normal force and bending," *Proc. of LABSE, Symposium on "Resistance and ultimate deformability of structures acted on by well defined repeated loads"*, Lisbon, Spain, 1973.

[6] Simulink®, The Mathworks, Inc., Natick, MA, USA. 2009.

[7] C.-P. Lamarche, A. Bonelli, O. Bursi, and R. Tremblay, "A Rosenbrock-W method for real time substructuring and PSD testing," *Earthquake Engineering and Structural Dynamics*, Vol. 38, no. 9, pp. 1071-1092, 2009.

[8] C.-P. Lamarche, R. Tremblay, P. Léger, M. Leclerc, and O. Bursi, "Comparison between real time dynamic substructuring and shake table testing techniques for nonlinear seismic applications," *Earthquake Engineering and Structural Dynamics*, DOI 10.1002/eqe.994, 2010.

[9] C. G. Broyden, "A class of methods for solving nonlinear simultaneous equations." *Math. Comput.*, Vol. 19, no. 92, 577–593, 1965.

[10] M. Ahmadizadeh, and G. Mosqueda, "Hybrid Simulation with Improved Operator-Splitting Integration Using Experimental Tangent Stiffness Matrix Estimation", *J. Struct. Engrg*. Vol. 134, no. 12, pp. 1829-1838, 2008.